Research Article | Vol. 29, No. 6 / 15 March 2021 / Optics Express 8283
Optics EXPRESS

Nonlinear signal errors in homodyne laser Doppler vibrometry induced by strong second-order ghost reflections and their mitigation

YANLU LI[1,2,*] AND ROEL BAETS[1,2]

[1] Photonics Research Group, Ghent University-imec, Technologiepark-Zwijnaarde 126, 9052 Ghent, Belgium
[2] Center for Nano- and Biophotonics, Ghent University, Technologiepark-Zwijnaarde 126, 9052 Ghent, Belgium
[*] Yanlu.Li@UGent.be

Abstract: A variety of mechanisms can induce distortions in the output signals of a homodyne laser Doppler vibrometer (LDV). In this paper, the nonlinear LDV distortions caused by a strong second-order ghost reflection originating from lens flares are theoretically explained and analyzed. We propose a simple compensation method to mitigate this distortion. The performance and limitations of this method are also explained both in simulation and in experiment.

1. Introduction

Laser Doppler vibrometry (LDV) is a non-contact vibration measurement method with picometer or even sub-picometer displacement resolution over a large frequency range [1], by taking advantage of the Doppler effect of a coherent light beam generated from a laser source. LDV has been used in many applications, such as aerospace [2], hearing [3], cardiology [4], rock fall risk evaluation [5], photo-acoustic imaging [6] etc. Nowadays, the most commonly used LDVs are based on discrete optics and fiber optics. These systems are usually not very compact. However, compactness is important for many applications that have a constrained space (e.g. implanted hearing aid) or require a limited weight (e.g. LDV carried by a drone). Based on this motivation, we have developed several compact LDV systems on a silicon-based photonic integrated circuit (PIC) [7,8]. For example, a packaged 6-beam LDV core with a laser source and an optical isolator has a footprint of 2.5×5 mm^2 [8]. Additionally, the cost of the PIC-based LDV sensors may also be strongly reduced for moderate or high volume productions thanks to the use of the CMOS compatible technologies [9]. A major difference between the current PIC-based LDV and conventional LDV is that the PIC LDVs are working in a homodyne mode while conventional LDVs usually use a frequency shifter to realize a heterodyne detection [10]. The frequency shifter is usually an acousto-optic modulator (AOM), and it is placed in one arm of the optical interferometer in the LDV to ensure a constant frequency difference between the measurement and reference signals. The frequency shift is often around tens of megahertz. The use of the frequency shifter can avoid the impact of low-frequency electronic noise (e.g. 1/f noise) and hence improve the sensitivity. However, the AOM is bulky and power-hungry, which is not compatible with applications that require very compact size and low power consumption. The frequency shifter also sets a boundary of the detection bandwidth in the heterodyne system. On the contrary, homodyne detection doesn't have such a carrier frequency, therefore it is much simpler and less power-hungry.

It is known that many factors, such as imperfect quadrature detectors, can cause nonlinear signal errors (quadrature fringes) in optical interferometry techniques such as LDV [11–13]. These distortions can be corrected with well-chosen post-processing algorithms. One common

#418439 https://doi.org/10.1364/OE.418439
Journal © 2021 Received 24 Dec 2020; revised 18 Feb 2021; accepted 22 Feb 2021; published 2 Mar 2021

Optics EXPRESS

correction method, reported by Heydemann [11], can correct most nonlinear errors originating from within the LDV itself (not related to the condition of the target). In this paper, we will discuss a different distortion mechanism induced by a ghost reflection from the lens that cannot be solved by the Heydemann correction. This distortion happens because some of the sensing optical beams travel between the lens and the device under test (DUT) multiple times before reaching the LDV receiver. As a result, the main reflection signal that is only reflected once by the DUT will be mixed with light beams that have reflected twice (second-order), three times (third-order) or more times from the DUT. Since the high-order ghost reflections have twice or more times the Doppler frequency shift in the main reflection, the corresponding errors in LDV signals will behave differently from the nonlinear errors handled by Heydemann correction. The nonlinear errors caused by these ghost reflections have been studied by Hu et al. [14–16], both in heterodyne and homodyne interferometers. They have developed several models to analyze the periodic nonlinearities originated from different orders of the ghost reflections. Based on these models, they analyzed the impacts of the ghost reflections on ultra-precision displacement measurement interferometers. In these systems, the ghost reflections are typically very weak. But there has been no report about the compensation algorithms to these errors.

In this paper, we will focus on the impacts of strong second-order ghost reflection on the homodyne PIC LDVs as well as on the compensation method to mitigate the problem. By "strong" second-order reflection, we mean that the optical powers of the second-order reflections are strong enough to distort the LDV signal significantly, but are still moderately lower than those of the main reflection (between 1% and 70%). These reflections usually appear when the DUT is not aligned to the image plane so that the main reflection is much weaker than the optimal value. One typical situation happens when the DUT is not fixed well. As the measurement time increases, the loose DUT may move away from the best-aligned location. When the second-order ghost reflection is directed to the sensor as a result of the DUT movement, the strength of the major reflection is usually also considerably reduced. In this case, the LDV signal will be distorted by the second-order ghost reflection. Based on the experience of the authors, this is not a rare phenomenon, but it may be ignored if the operators don't check the updated IQ circles frequently. Our method can compensate for these distortions after the measurements, so as to avoid the repetition of some measurements which are difficult or time-consuming to realize. Theoretically, the compensation method can work for very weak second-order ghost reflections (<1%). However, deviations can be introduced by some algorithms used in the current compensation code, which makes it not practical for compensating signals with very weak reflections.

In most cases, especially when the DUT surface diffuses light, the strengths of third- and higher-order ghost reflections are much weaker than the second-order ghost reflection, since higher-order ghost reflections experience more times of diffusing. As we will explain later in this paper, the distortion phenomena of the second-order ghost reflection are different from those of the higher-order ghost reflections. Based on the difference, we can tell that most non-linear deviations in our measurements are mainly associated with the second-order ghost reflection. Therefore, compensation algorithms for higher-order reflections, which are generally more complicated, are not required in these cases.

We will briefly introduce the working principle of the homodyne PIC LDV and the impact of a strong second-order ghost reflection in section 2. In section 3, the compensation method will be introduced and the corresponding performance will be theoretically studied. In Section 4, an experiment that demonstrates the existence of the second-order reflection and the performance of the compensation method will be explained. The final part is the conclusion.

Optics EXPRESS

2. Working principle of the homodyne LDV and different distortion mechanism

The basic configuration of a homodyne PIC LDV is a laser interferometer (typically a Mach-Zehnder interferometer) with one arm used for vibration signal retrieval (see Fig. 1(a)). Light generated from the laser source is sent to the interferometer fabricated in the PIC and is split into two parts by an optical splitter. One part is the measurement signal which is sent to the DUT and which retrieves its movement information according to the Doppler effect, while the other part is the reference signal, which is mixed with the reflected measurement signal to generate an intensity change (beating effect) via an optical combiner. The photocurrent of the photodiode (PD) that receives the combined optical signal is expressed as

$$I_{pd}(t) = \frac{\eta}{4}\left(|a|^2 + \mu^2|b|^2 + 2\mu ab \cdot \cos(\theta(t) + \theta_0)\right),$$

where η represents the responsivity of the PD, a and b represent the phasor amplitudes of the reference signal and measurement signal (before sending out from the LDV), respectively, μb is the amplitude of the reflected signal collected by the LDV receive antenna, $\theta(t)$ is the Doppler phase shift introduced by the movement of the target, and θ_0 is the constant phase difference between the reference and measurement signals. In the on-chip homodyne LDV, the optical combiner for the reflection and reference signals is usually realized by a 90-degree optical hybrid [17] with four unique PDs connected to its four outputs [7]. With this combiner, one can obtain four signals, with $\theta_0 = \theta_{const} + k\pi/2$, $k = 1, 2, 3, 4$. By obtaining the difference of the two PDs with opposite phases (i.e. pair 1: $k = 1$ and $k = 3$, pair 2: $k = 2$ and $k = 4$), one can get two signals which are called I and Q signals:

$$I(t) = \eta\mu ab \cdot \cos\left(\theta(t) + \theta_{const}\right),$$
$$Q(t) = \eta\mu ab \cdot \sin\left(\theta(t) + \theta_{const}\right).$$

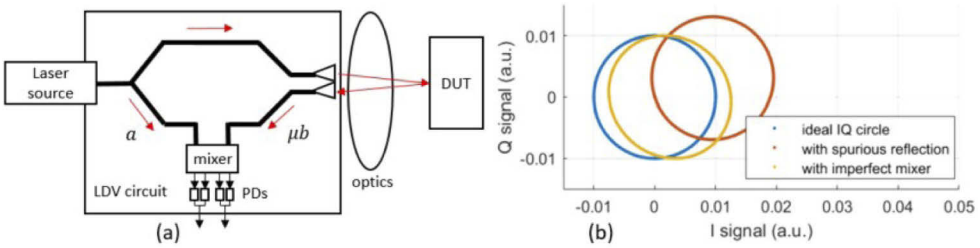

Fig. 1. (a). The configuration of a typical homodyne PIC LDV. (b) the Lissajous curve of I and Q signals with different distortions. Blue: no distortion; red: with DC drift; orange: with phase errors and imbalanced responsivities in PDs.

The Lissajous curve of the IQ signals is an important tool to understand the performance of a homodyne LDV. An ideal IQ curve is a circle with the center on the origin of the coordinate system (blue curve in Fig. 1(b)). The phase of each point of the IQ curve is $\theta(t) + \theta_{const}$, which corresponds to the Doppler phase change in the measurement arm. The radius of the IQ circle equals $\eta\mu ab$, which can be used to estimate the measurement signal reflection strength $(\mu b)^2$.

Many distortions can be directly seen in the IQ circle. For example, the spurious reflection from on-chip antennas or lenses or imbalance in the PD responsivities can cause a DC drift of the IQ curve. The red curve in Fig. 1(b) shows an IQ curve with a spurious reflection that has the same amplitude as the reflection signal (the phase of the spurious reflection is set as $\pi/4$). Another common problem is that the IQ circle is an ellipse instead of a circle. This is generally caused by the phase errors in the 90-degree optical hybrid or uneven responsivities of PDs. The

Optics EXPRESS

orange curve in Fig. 1(b) shows an IQ curve with 5° phase errors in both I and Q channels and 1% responsivity change in one of the PDs. In these plots, we assume $\mu b = 0.01 \times a$. These errors can be compensated with the Heydemann correction. Generally speaking, the Heydemann correction uses a least-square fitting algorithm to find the eccentricity, center, and rotation angle of the ellipse. With these parameters, we can calculate the corrected I and Q signals without distortions [7]. Note that the change of laser wavelength can also impact the phase errors of the optical hybrid [17]. Therefore, if the wavelength changes during the measurement, one needs to redo the Heydemann correction frequently for long signal recovery.

However, in some measurements, e.g. when the target a diffusing aluminum surface, it is found that the IQ curve is not a circle, but a cardioid (see Fig. 2(a)). As a result, the demodulated signal of the LDV will have extra errors because of this IQ shape [15]. It is also found that the shape of the IQ curve changes as the location of the DUT and the rotation angle of the lens change, which means it is not a phenomenon that is only associated with the LDV circuit itself. This effect is actually caused by the reflections that travel twice between the sensor and the DUT (second-order ghost reflection). The optical lens that is used to focus light on the target may not be perfectly anti-reflective. Additionally, the boundaries of the lens also scatter light reflectively. As a result, some part of the light that has been reflected by the DUT once can be sent back to the DUT again (see Fig. 2(b)) and is then sent to the LDV receiving antenna. The second-order ghost reflection carries a phase shift of $2\theta(t)$ and is mixed with the main reflection. Similarly, there are also third- and higher-order ghost reflections. The ghost reflections are not significant when the DUT is at the image plane of the antenna, in which case the main reflection is very strong and dominant. But they become much stronger and clearer when the DUT moves away from the best reflection location, being the image plane.

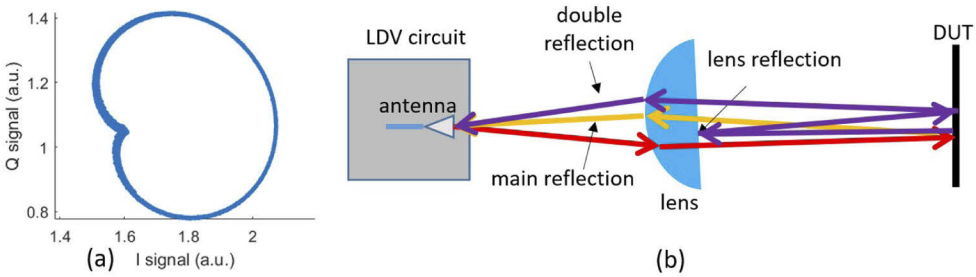

Fig. 2. (a) A measured IQ curve that looks like a cardioid. (b) The cause of the cardioid IQ curve: second-order ghost reflection by the lens-air interface.

Now we only consider the second-order reflection, the phasor of the reflection signal can be described as

$$I(t) + j \cdot Q(t) = \eta\mu_1 ab \cdot \exp(j\theta(t)) + \eta\mu_2 ab \cdot \exp(j2\theta(t) + j\theta_2) \tag{1}$$

where $\mu_1 b$ and $\mu_2 b$ are the phasor amplitudes of the main reflection and second-order ghost reflection, respectively, and θ_2 is the phase difference between the second-order ghost and main reflections. Depending on the ratio between the second-order and the main reflections, the shape of the IQ curve varies (Fig. 3(a)). The rotations of the IQ curves are determined by the phase difference θ_2 (Fig. 3(b)).

The IQ curve can be fully described by a shifted Limaçon curve. Like a Limaçon, the shape of the IQ curve has different types: when μ_2/μ_1 is between 0 and 0.25, the shape is a dimpled Limaçon (purple plot in Fig. 3(a)); when μ_2/μ_1 is between 0.25 and 0.5, the shape becomes a cusp (orange plot in Fig. 3(a)); it is a cardioid when $\mu_2/\mu_1 = 0.5$; when μ_2/μ_1 is larger than 0.5, the shapes will become looped and hence have a crossing point (blue and red plots in Fig. 3(a)).

Optics EXPRESS

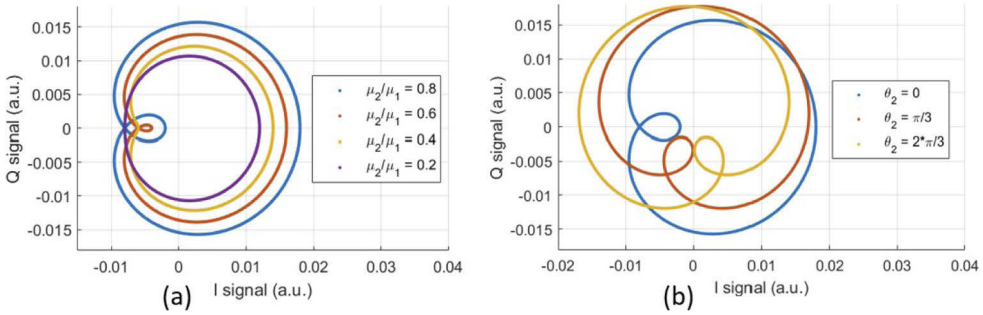

Fig. 3. Plots of the IQ curves based on the Eq. (1). (a) The IQ curves of LDV signals with a second-order ghost reflection with different strengths (b) The IQ curves of LDV signals with different phases (θ_2) between the main reflection and the second-order ghost reflection when $\mu_2/\mu_1 = 0.8$. In all plots, it is assumed that $\mu_1 b/a = 0.01$.

We can see that it is difficult to notice the impact of the second-order ghost reflection when μ_2/μ_1 is less than 0.25. When the main reflection is weak because of defocusing, the second-order ghost reflection can be relatively strong. All these shapes can easily be found in real experiments.

The demodulated signals with different μ_2/μ_1 values are shown in Fig. 4(a). It can be seen that the error values are different for different displacements. The impact of the second-order ghost reflection can be estimated by the root-mean-square (*rms*) error of the demodulated signal w.r.t. the original signal, which is defined as $dev = rms(\theta_{demo}(t) - \theta(t))$, where $\theta_{demo}(t)$ is the demodulated phase of the signal and $\theta(t)$ is the actual phase caused by the movement of the target. In Fig. 4(b), we show the error values for different μ_2/μ_1 ratios for a 50 Hz sinusoidal vibration signal with different amplitudes (half-amplitude A_h = 2 μm, 4 μm, 6 μm, 8 μm and 10 μm.). The wavelength used for sensing is $\lambda = 1550nm$. The internal LDV errors are assumed to be absent in these simulations. It can be seen that the phase error increases with the μ_2/μ_1 value. From the data in Fig. 4(b), we estimate that the standard deviation of the error values, in this case, is less than 1.5% for different vibration amplitudes, providing that the vibration amplitudes are much larger than half of the laser wavelength. For vibrations with small amplitudes, the error values will depend on the constant phase difference θ_{const}. Currently, the errors are shown

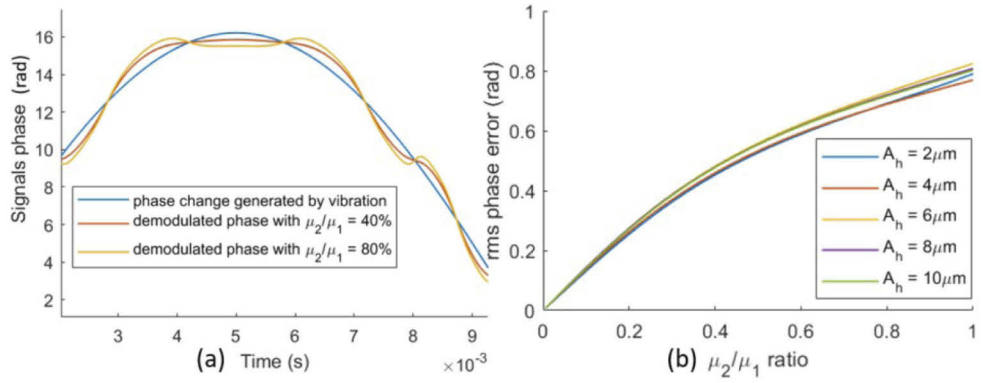

Fig. 4. Simulated signal errors caused by the second-order ghost reflection based on Eq. (1). (a) Demodulated signal error for two different μ_2/μ_1 ratios. (b) The phase errors of the demodulated signal as a function of the μ_2/μ_1 ratio, for vibrations with half-amplitude A_h = 2 μm, 4 μm, 6 μm, 8 μm and 10 μm. The wavelength of the sensing signal is 1550 nm.

Optics EXPRESS

as phase errors with the unit of rad. To convert them to displacement errors, one can use the formula derived from the Doppler effect $d(t) = \lambda\theta(t)/4\pi$. For example, a phase error of 0.1 rad corresponds to a displacement error of 12.3 nm.Besides the second-order ghost reflection, there can also be third- or high-order reflections. Compared to the second-order reflection, a third-order reflection leads to a different and more complicated shape in the IQ curve. Several examples are shown in Fig. 5(a), where the phasor amplitudes of the third-order ghost reflection are represented by $\mu_3 b$. When the target is a mirror, there is a great chance to find strong third- or high-order ghost reflections. However, if the target is a diffuse reflector, which is the case in a lot of LDV applications, the loss of each round trip between the lens and the DUT is much higher. As a result, the strengths of the third- or higher order-reflections will be much weaker than that of second-order reflection. We will focus on the situation where only second-order ghost reflections are dominant, so the third and high-order ghost reflections will not be discussed further in this paper.

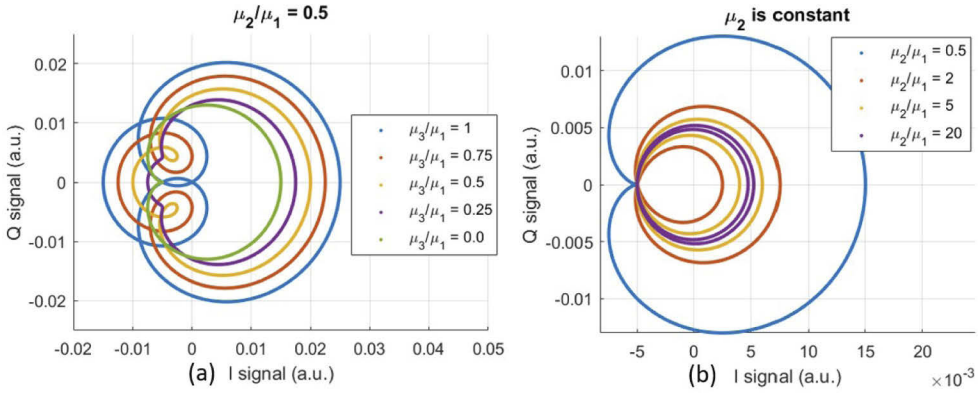

Fig. 5. Plots of the IQ curves calculated based Eq. (1). (a) The IQ curves with both second- and third-order ghost reflections. A third-order reflection $\eta\mu_3 ab \cdot \exp(j3\theta(t))$ is added to Eq. (1). It is assumed that $\mu_3/\mu_1 = 0.5$. (b) The IQ curves when the ratio of the second-order ghost reflection and the main reflection becomes stronger while μ_2 is kept constant.

One thing to notice is that the strength of the second-order reflection can be much stronger than the main reflection in some special cases. That usually happens in a situation that the main reflection is strongly defocused and thus becomes quite weak. As is seen in Fig. 5(b), the region encircled by the crossed part of the IQ curve becomes larger as μ_2/μ_1 ratio increases. When μ_2/μ_1>5, we may mistakenly calculate the Doppler phase change to be twice the expected value. It is difficult to notice this error if it exists during the entire period of the measurement. However, if a good alignment is made at the beginning of the measurement, it is possible to identify the evolution of this error and remove its corresponding impact.

The zero-order reflection is the reflection directly reflected from the optics back to the LDV circuit, so it doesn't have any Doppler frequency shift. Therefore, the zero-order reflection is considered as a part of the spurious reflection, and it can be compensated with Heydemann correction.

3. Compensation algorithm for a strong second-order ghost reflection

To compensate for the errors caused by a strong second-order ghost reflection, one needs to figure out the values of $b_1 = \eta\mu_1 ab$ and $b_2 = \eta\mu_2 ab$. The IQ signals are usually not able to be expressed as Eq. (1) because of various problems, such as the difference in PD responsivities, spurious reflections (zero-order ghost reflection), and phase errors in the 90-degree optical hybrid. These problems will lead to DC drifts and zero-order shape distortions of the IQ curve similar to what

Optics EXPRESS

is shown in Fig. 1(b). When there is no DC drift and zero-order shape distortions in the IQ curve, the IQ signals that are distorted by the second-order ghost reflection can be expressed as in Eq. (1). Then, it is possible to retrieve the values of b_1, b_2 and θ_2 by solving the following equation using the measured I and Q data

$$R^4 - R^2 \cdot (b_1^2 + 2b_2^2) - 2b_2 b_1^2 I\cos(\theta_2) - 2b_2 b_1^2 Q\sin(\theta_2) + (b_2^2 - b_1^2)b_2^2 = 0 \tag{2}$$

In this equation, $R^2 = I^2 + Q^2$. This equation can be solved using numerical methods, such as linear fitting. However, if there is an unknown DC drift or shape distortion, solving the aforementioned equation is not an easy task. We propose a different method, based on the fact that the IQ curve is axisymmetric. Note that the IQ shape in Fig. 2(a) is not completely axisymmetric, which is caused by zero-order shape distortion originated from the internal phase errors in the LDV. So we use the Heydemann correction to correct the IQ curve first. Then we need to find the symmetric axis of the IQ curve. This can be done by measuring the width of the IQ curve (see Fig. 6(a)) as a function of the rotation angle. The rotation is realized by multiplying the IQ data with a series of rotation matrices

$$M_r(\alpha) = \begin{bmatrix} cos(\alpha) & -sin(\alpha) \\ sin(\alpha) & cos(\alpha) \end{bmatrix} \tag{3}$$

with different rotation angles α ranging from 0 to 2π. One example of the width versus the rotation angle is seen in Fig. 6(b). In this simulation, the value of θ_2 is set as 50°.

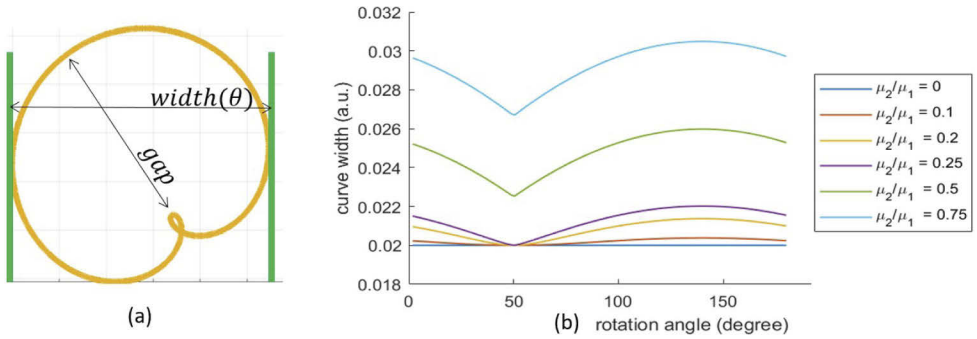

Fig. 6. Plots based on mathematical calculations. (a) The width and gap of an IQ curve deviated by the second-order ghost reflection. (b) The width of the IQ curve as a function of rotation angle for different μ_2/μ_1 values with $\theta_2 = 50°$ for all signals.

It can be seen from Fig. 6(b) that the width has a minimum at the rotation angle of 50° (Fig. 6(b)) and a maximum value at 140°. The minimal width values are the same as the gap when μ_2/μ_1<0.25. These are the cases when the IQ curve is a dimpled Limaçon curve. According to Eq. (1), the gap value equals $I(0) - I(\pi) = 2b_1$. When μ_2/μ_1>0.25, the shape of the IQ curve starts to become like a cardioid, therefore the minimum width will be larger than $2b_1$.

After obtaining the rotation angle, we will rotate the curve back to the normal direction ($\theta_2 = 0$) by using a proper rotation matrix. As a result, the symmetric axis of the rotated curve is $Q = (max(Q(t)) + min(Q(t))/2$, where $max(Q(t))$ and $min(Q(t))$ are the maximal and minimal values of the Q values, respectively. Then the entire IQ curve is moved so as to be symmetric to the axis $Q = 0$. This is done by subtracting all Q values with $(max(Q(t)) + min(Q(t)))/2$. In this new curve, the value gap can be easily retrieved. Therefore, we can obtain the value of b_1.

Optics EXPRESS

To obtain the values of b_2 and I_c, we will take advantage of two special points on the IQ curve (Fig. 7),

$$[I(\pi/2), Q(\pi/2)] = [I_c - b_2, b_1]$$
$$[I(\pi), Q(\pi)] = [I_c - (b_1 - b_2), 0].$$

The coordinates of these two positions can be retrieved from the IQ curve since their Q values are already known. Then we have

$$I_c = \frac{b_1 + I(\pi) + I(\pi/2)}{2},$$
$$b_2 = \frac{b_1 + I(\pi) - I(\pi/2)}{2}.$$

To retrieve the undistorted Doppler phase shift, we can form a vector based on the obtained parameters

$$(I(t) - I_c) + j(Q(t) - Q_c) = (b_1 + 2b_2\cos(\theta(t))) \cdot \exp(j\theta(t)), \tag{4}$$

where $Q_c = 0$. The value of $\theta(t)$ can be derived from the angle of this vector. However, when $b_2 > b_1/2$, the magnitude of the vector $|b_1 + 2b_2\cos(\theta(t))|$ can become zero when $\cos(\theta(t)) = -b_1/2b_2$. This situation corresponds to the location where the IQ curve crosses (see Fig. 7). To retrieve the right phase $\theta(t)$, one needs to change the sign of the demodulated signal when the IQ signal crosses this point. However, it is still easy to have a phase jump in the demodulated signal at this spot, especially when noise is present. We remove the distortion from these crossing points by deleting the demodulated values at these positions and regenerate the signal by extrapolating from the adjacent data.

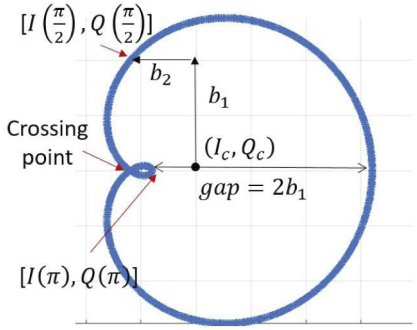

Fig. 7. The two special points in a typical IQ curve corrupted by second-order reflections and the crossing point of the curve when $\mu_2/\mu_1 > 0.5$.

The effects of signal compensation are simulated for two cases ($\mu_2/\mu_1 = 0.4$, $\mu_2/\mu_1 = 0.8$) and shown in Fig. 8. It can be seen that the compensation algorithm works well when there is no noise. Nevertheless, for the case with $\mu_2/\mu_1 = 0.8$, we still see several sharp spikes in the demodulated signal with compensation algorithm (e.g. red curve at t = 0.004s). These spikes are caused by the errors associated with the crossing points of the IQ curves. The error of the demodulated signal with compensation as a function of μ_2/μ_1 is shown in Fig. 9(a). It can be seen that the compensation works well when $\mu_2/\mu_1$is between 0.04 and 0.84. When $\mu_2/\mu_1 < 0.04$, the IQ curve is very similar to a circle and our proposed demodulation may introduce errors in these situations. For $\mu_2/\mu_1 > 0.84$, the distortions associated with the big inner-loops of the IQ curves are not well corrected. A better algorithm to remove those distortions is required. For the region between 0.04 and 0.84, the compensation works well and it can suppress the phase error less than 0.05 rad (6 nm).

Optics EXPRESS

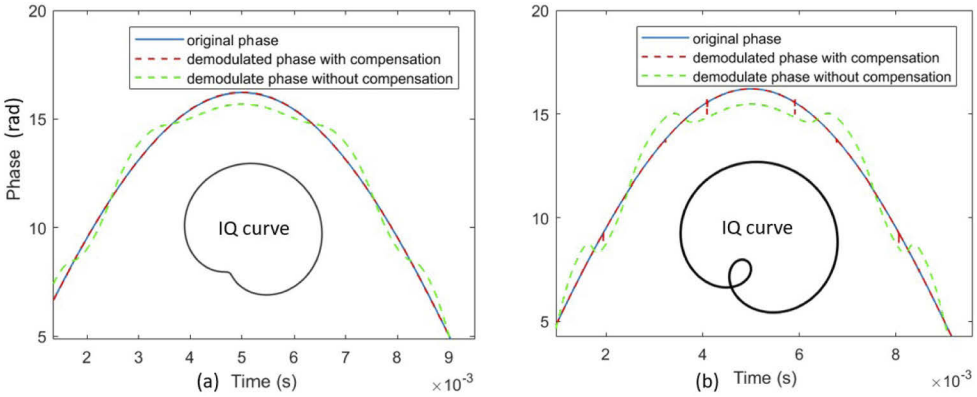

Fig. 8. Simulation of the demodulated signal with/without compensations. (a) Comparison of the demodulated signals between with and without compensations, for $\mu_2/\mu_1 = 0.4$. (b) Comparison of the demodulated signals between with and without compensations, for $\mu_2/\mu_1 = 0.8$. The original vibration is a sinusoidal signal with a frequency of 50 Hz and a half-amplitude of 2 μm.

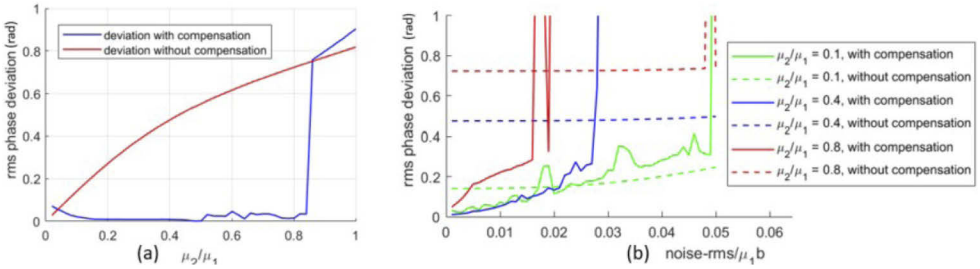

Fig. 9. Simulated rms phase deviations. (a) The phase error of the demodulated signal w.r.t. the original signal for the case with and without compensation (without noise). (b) the phase error of the demodulated signal w.r.t. the original signal with different noise levels.

The compensation method, however, can be impacted by noise. In Fig. 9(b) we plotted the error of the demodulated signals with different levels of noise. It can be seen that for all simulated cases, the compensation works when the average noise amplitude is less than 1.5% (-36dB) of the amplitude of $\mu_1 b$. When the noise gets stronger, the phase jumps in the compensation method is the dominant factor for the nonlinear error.

4. Experiment

To show the presence of the second-order reflection in the measurement and the performance of the compensation method, we did experiments with our on-chip homodyne LDVs [8]. The LDV PIC has six LDV channels with an antenna spacing of 0.3 mm. We only use two of the LDV channels (Fig. 10(a)). We use one plano-aspheric lens with anti-reflective coatings (A220-TMC, the plano surface facing the DUT) to focus the output beam to a gold mirror with an optical magnification of around 2 (Fig. 10(b)). Since the two measurement locations on the mirror are quite close to each other (approximately 0.6 mm), we can assume that their received signals are very similar. However, the amplitudes of the second-order ghost reflections to these two LDVs can be different. We can adjust the system and enable a case in which there is strong second-order ghost reflection to LDV 2 while the second-order ghost reflection to LDV 1 is very weak. The laser source is a distributed-feedback (DFB) laser working at 1550 nm, with an output power of

Optics EXPRESS

around 5.5 mW shared by the six LDVs. The vibration is generated by a piezoelectric (PZT) stack glued to the back of the mirror. The peak-to-peak driving voltage is 20 V across the PZT, and the frequency is 1 kHz. The sampling rate of the LDVs is 100 ksps.

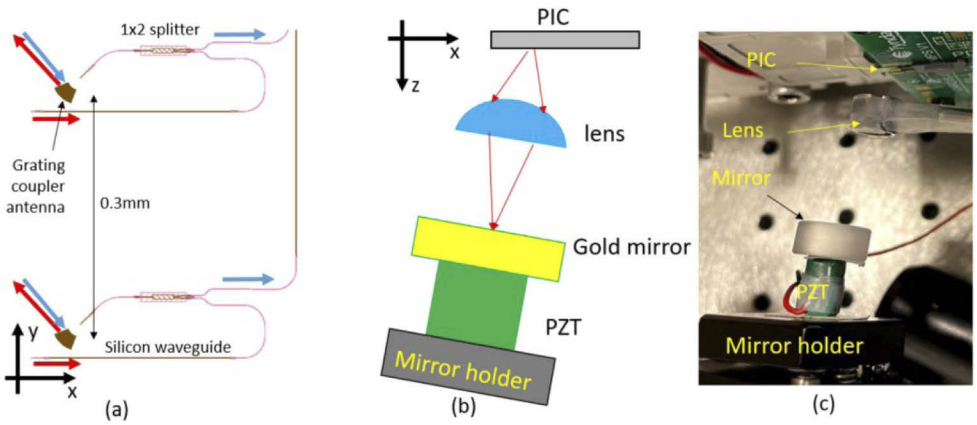

Fig. 10. (a) The antennas of the dual LDV design, red curves stand for outgoing light and blue curves stand for reflection light. (b) Schematic of the measurement setup to show the second-order ghost reflection. (c) A picture of the measurement setup.

By adjusting the direction and the position of the mirror, one can change the reflection conditions to both of the LDV antennas. It can be seen that when the reflection is strong (large IQ curve), both IQ curves look like ellipses without the distortions induced by ghost reflections. One such example is seen in Fig. 11(a). The IQ shape is not distorted by ghost reflections because the system is well focused and the main reflections are dominant. The ellipse shape is caused by the internal LDV distortions, as mentioned earlier. We registered the information of the two ellipses and use them to correct the internal phase errors for the other cases. When the reflection is weaker (small IQ curve), we noticed that the shapes of the IQ circles change easily as the rotation of the mirror changes. One example is seen in Fig. 11(b), which is from the same beam. Note that the size of IQ circle in Fig. 11(b) is smaller than that in Fig. 11(a). From the shapes of these IQ plots we can tell that many distortions are caused by the second-order reflection. After careful adjustment, we can find one situation in which the IQ curve for LDV 1 has an ellipse shape (very weak second-order ghost reflection) while the one for LDV 2 has a Limaçon shape (strong second-order ghost reflection). Both IQ curves are then phase-error corrected with Heydemann correction by using the information obtained from the undistorted large IQ ellipses. The corrected IQ curves are shown in Fig. 11(c) and Fig. 11(d), respectively. The Limaçon shape in Fig. 11(c) corresponds to the one shown in Fig. 11(b). It can be noticed that the shape of Fig. 11(c) is more symmetric than the one shown in Fig. 11(b) since it has been corrected by using the Heydemann correction. All the IQ plots are for a time slot of 0.05 s. Within this time slot, the IQ data travel around the center of the curve more than 100 times. Since the reflection strength may change during the period of measurement, the thickness of the IQ curve can be broadened as a result.

Then we used our proposed compensation method to recover the original signal of the distorted shape. Note that we measured the signal from LDV 1 and LDV 2 at the same time, while the signal from LDV 1 should be undistorted judging from the ellipse shape of the IQ curve. Therefore, we assume that the demodulated signal of LDV 1 is the same as the undistorted signal of the LDV 2. In Fig. 11(e), we plot the difference of the demodulated displacements between LDV 2 (for the cases with and without compensation) and LDV 1 (without compensation). It can be seen that the displacement error of the demodulated signal from LDV 2 to that of LDV 1 in the

Optics EXPRESS

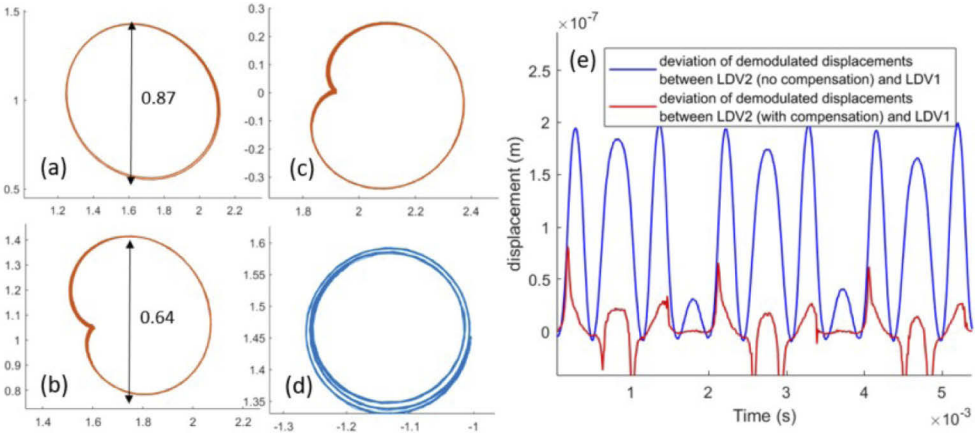

Fig. 11. Measurement results showing the impact of ghost reflections and compensations. (a) The IQ curve for LDV 2 when there is a strong main reflection and a weak second-order ghost reflection. (b) The distorted IQ curve for LDV 2 when there is a relatively weak main reflection and a strong second-order reflection. (c) The Heydemann corrected IQ curve for LDV 2 data shown in figure b. (d) The Heydemann corrected the IQ curve for LDV 1, which should have a very weak second-order reflection. (e) The deviations of the demodulated displacements for LDV 1 (without compensation) and LDV 2 (with and without compensation)

case of without compensation is around 107 nm, while this error value becomes approximately 20 nm when we use the compensation method for LDV 2. Impact of noise may be the reason why the compensated LDV 2 is not perfectly matched to that of LDV 1. These results show that the compensation method works for these strong second-order ghost reflections.

The estimated deviation values of a series of experimental results with different μ_2/μ_1 ratios are converted to phase deviations and are shown in Fig. 12. Since we cannot always find undistorted signals (e.g. LDV1 data shown in Fig. 11) to compare for all these measurements, we use the root-mean-square phase fluctuations corresponding to the high-order harmonics (except the fundamental harmonic) in the demodulated signals. These estimated deviations are similar to the

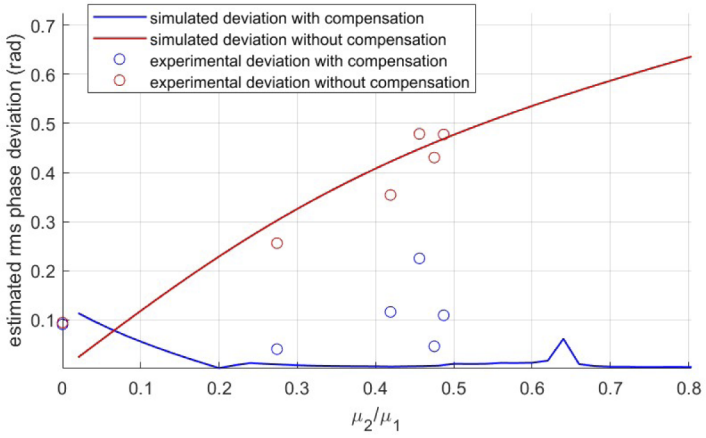

Fig. 12. Estimated deviations for compensated measurement data and simulation data as a function of μ_2/μ_1 ratio.

Optics EXPRESS

real deviations when the original vibration signal has negligible power in high-order harmonics, which is the case for these measurements. The simulated deviations obtained using the same estimated method are also shown in the same figure. It can be seen that the deviations caused by the second-order ghost reflections can be reduced by using our proposed compensation method when $\mu_2/\mu_1>0.1$. The working range of μ_2/μ_1 is different from the result in Fig. 9(a) because the half-amplitude of the vibration in this simulation is reduced to 0.6 μm, which is set to be similar to the measured values. Since this amplitude is very close to the laser wavelength, the error of algorithms (especially the one used to find the symmetric axis) in the compensation code increases dramatically when μ_2/μ_1 becomes small (becomes more like a circle). It is also seen that the compensated values for the experimental results are not as good as the simulated values, that's because the simulation doesn't consider the impact of noise. Noise can increase the errors of various algorithms in the code, which makes the compensation code less effective.

5. Summary and discussion

In this paper, we have analyzed the nonlinear signal errors introduced by the second-order ghost reflection from the DUT. Though some papers have analyzed the impacts of these ghost reflections, no compensation method has been reported, especially for relatively strong second-order ghost reflections. A simple compensation method is proposed in this paper. The compensation algorithm works in a situation where the second-order ghost reflection is relatively strong but still moderately weaker than the main reflection, while other orders are negligible. In most cases when the target is a diffuse reflector, the third- and higher-order ghost reflections are usually very weak. Therefore, the proposed method can help to recover the signal distortions in a lot of situations.

When no noise is considered, our current algorithm works well for signals with the μ_2/μ_1 ratio lying between 0.1 and 0.84. Currently, the upper limit of the μ_2/μ_1 is caused by algorithms used to search for the special points in the IQ curves (see Fig. 7), which don't work well for IQ curves with a big inner loop. The lower limit may be associate with the symmetric-axis finding algorithm, which will be less accurate when the IQ curve approaches a nice circle. When noise exists, the performance of this method can deteriorate, but it still improves the signal quality. Another challenge with this method is that relatively strong phase jumps can happen at the crossing points of the IQ curves, which exist when $\mu_2/\mu_1>0.5$. These jumps can be partially removed with simple algorithms, but not completely. We believe better algorithms can be developed in the future to further reduce the impacts of those jumps.

In conclusion, the current compensation method can effectively reduce nonlinear errors introduced by second-order reflections within a certain power range. Some of the algorithms in the compensation method should be further improved so that this method can be less sensitive to noise and work for an even larger reflection range.

Funding. European Union's Horizon 2020 Framework Programme CARDIS project (644798).

Disclosures. The authors declare no conflicts of interest.

References

1. M. Johansmann, G. Siegmund, and M. Pineda, "Targeting the limits of laser Doppler vibrometry," in "*Proceedings of the International Disk Drive Equipment and Materials Association 2005* (International Disk Drive Equipment and Materials Association, 2005)," 1–12 (2005).
2. L. Jacquin, D. Fabre, D. Sipp, V. Theofilis, and H. Vollmers, "Instability and unsteadiness of aircraft wake vortices," Aerosp. Sci. Technol. **7**(8), 577–593 (2003).
3. K. Whittemore, S. Merchant, B. Poon, and J. Rosowski, "A normative study of tympanic membrane motion in humans using a laser doppler vibrometer (LDV)," Hear. Res. **187**(1-2), 85–104 (2004).
4. Y. Li, L. Marais, H. Khettab, Z. Quan, S. Aasmul, R. Leinders, R. Schüler, P. Morrissey, S. Greenwald, P. Segers, M. Vanslembrouck, R. Bruno, P. Boutouyrie, P. O'Brien, M. de Melis, and R. Baets, "Silicon photonics-based laser Doppler vibrometer array for carotid-femoral pulse wave velocity (PWV) measurement," Biomed. Opt. Express **11**(7), 3913–3926 (2020).

Optics EXPRESS

5. F. Uehan, "Rockfall risk evaluation system with laser & drone measurement," Jpn. Railway Eng. **196**, 2–5 (2017).
6. L. Mignanelli and C Rembe, "Feasibility study of the employment of laser Doppler Vibrometry for photoacoustic imaging," J. Phys.: Conf. Ser. **1149**, 012028 (2018).
7. Y. Li and R. Baets, "Homodyne laser Doppler vibrometer on silicon-on-insulator with integrated 90 degree optical hybrids," Opt. Express **21**(11), 13342–13350 (2013).
8. Y. Li, J. Zhu, M. Duperron, P. O'Brien, R. Schüler, S. Aasmul, M. De Melis, M. Kersemans, and R. Baets, "Six-beam homodyne laser Doppler vibrometry based on silicon photonics technology," Opt. Express **26**(3), 3638–3645 (2018).
9. W. Bogaerts, R. Baets, P. Dumon, V. Wiaux, S. Beckx, D. Taillaert, B. Luyssaert, J. Van Campenhout, P. Bienstman, and D. Van Thourhout, "Nanophotonic waveguides in silicon-on-insulator fabricated with CMOS technology," J. Lightwave Technol. **23**(1), 401–412 (2005).
10. R. Kowarsch and C. Rembe, "Heterodyne interferometry at ultra-high frequencies with frequency-offset-locked semiconductor lasers," Meas. Sci. Technol. **31**(7), 075201 (2020).
11. P. Heydemann, "Determination and correction of quadrature fringe measurement errors in interferometers," Appl. Opt. **20**(19), 3382–3384 (1981).
12. C. Wu and C. Su, "Nonlinearity in measurements of length by optical interferometry," Meas. Sci. Technol. **7**(1), 62–68 (1996).
13. T. Eom, J. Kim, and K. Jeong, "The dynamic compensation of nonlinearity in a homodyne laser interferometer," Meas. Sci. Technol. **12**(10), 1734–1738 (2001).
14. P. Hu, Y. Bai, J. Zhao, G. Wu, and J. Tan, "Toward a nonlinearity model for a heterodyne interferometer: not based on double-frequency mixing," Opt. Express **23**(20), 25935–25941 (2015).
15. P. Hu, Y. Wang, H. Fu, J. Zhu, and J. Tan, "Nonlinearity error in homodyne interferometer caused by multi-order Doppler frequency shift ghost reflections," Opt. Express **25**(4), 3605–3612 (2017).
16. H. Fu, Y. Wang, P. Hu, J. Tan, and Z. Fan, "Nonlinear Errors Resulting from Ghost Reflection and Its Coupling with Optical Mixing in Heterodyne Laser Interferometers," Sensors **18**(3), 758 (2018).
17. R. Halir, G. Roelkens, A. Ortega-Monux, and J. Wanguemert-Perez, "High performance 90° hybrid based on a silicon-on-insulator multimode interference coupler," Opt. Lett. **36**(2), 178–180 (2011).